Accepted Manuscript

Effective elastic thickness in the Central Andes. Correlation to orogenic deformation styles and lower crust high-gravity anomaly

Héctor Pedro Antonio García, Gianni Guido, Lupari Marianela, Sánchez Marcos, Soler Santiago, Ruiz Francisco, Lince Klinger Federico

PII: S0895-9811(17)30310-3

DOI: 10.1016/j.jsames.2017.11.021

Reference: SAMES 1843

To appear in: *Journal of South American Earth Sciences*

Received Date: 31 July 2017

Revised Date: 25 November 2017

Accepted Date: 27 November 2017

Please cite this article as: Antonio García, Hé.Pedro., Guido, G., Marianela, L., Marcos, Sá., Santiago, S., Francisco, R., Federico, L.K., Effective elastic thickness in the Central Andes. Correlation to orogenic deformation styles and lower crust high-gravity anomaly, *Journal of South American Earth Sciences* (2017), doi: 10.1016/j.jsames.2017.11.021.

Effective Elastic Thickness in the Central Andes. Correlation to orogenic deformation styles and lower crust high-gravity anomaly

Héctor Pedro Antonio García[a,b,*], Gianni Guido[a,b], Lupari Marianela[a,b], Sánchez Marcos[a,b], Soler Santiago[a,b], Ruiz Francisco[a,b], Lince Klinger Federico[a,b]

[a] *Consejo Nacional de Investigaciones Científicas y Técnicas (CONICET) Argentina*
[b] *Instituto Geofísico Sismológico Ing. Volponi. Facultad de Ciencias Exactas, Físicas y Naturales, Universidad Nacional de San Juan, Ruta 12, km 17, C.P. 5407, Jardín de los poetas, Marquesado, Rivadavia, San Juan, Argentina*

Abstract

Global studies have assessed the importance of elastic thickness (T_e) on orogenic evolution, showing that the style and nature of upper crustal shortening are influenced by the inherited lithospheric strength. Thus, pioneer works have identified that the upper crustal deformation style in the easternmost sector of the Central Andes in South America are related to the elastic thickness (T_e). There, the thick-skinned and pure-shear style of Santa Bárbara system was initially related to the existence of low T_e values. In contrast, the thin-skinned and simple-shear style of deformation in the Subandean system involves high T_e values. However, more recent T_e studies in the Central Andes present conflicting results which lead to question this straightforward relation. Results from these studies show a strong dependence on the applied methodology hampering the general understanding of the lithospheric thermo-mechanical state of the Central Andes. To contribute to this issue, we perform a high-resolution T_e map, using forward modeling by solving flexural equation of infinite plate model in two dimensions. To achieve this, the crust-mantle interface was calculated using a high-resolution gravity anomaly dataset which combines satellite and terrestrial data, and an average density contrast. Additionally, the gravity anomaly and the foreland basin depth in the Central Andes were best predicted by considering that lower crustal rocks fill the space deflected downward in the plate model. The obtained T_e values show an inverse correlation with previous heat flow studies, and a

*Corresponding author
Email address: garciahectorantonio@gmail.com (Héctor Pedro Antonio García)

strong spatial correlation with the styles and mechanisms of deformation in the easternmost sector of the Central Andes. In the Santa Bárbara system T_e values less than 10 km predominate, whereas in the Subandean system high T_e values were observed. Such high values correlate with the orogenic curvature and with an shallower gravity Moho zone, which breaks the regional trend of the Central Andes. This shallower gravity Moho is linked to a high-gravity anomaly located in the east part of the Eastern Cordillera and Subandean system. These results are also correlated with a high-velocity zone in the upper mantle previously found by receiver functions studies. This correlation could indicate changes in the properties of the lower crustal rocks that justify the shallower gravity Moho zone and explain in part the highest T_e values.

Keywords: `Elastic Thickness, Central Andes, Deformation Style, Gravity Moho`

1. Introduction

Plate tectonics theory suggests that the lithosphere can be divided into a number of plates that have remained relatively rigid for long periods of time (Watts and Burov, 2003). The properties of the lithosphere govern the deformation and dynamics of tectonic plates (Kirby, 2014). The flexural rigidity (D) is one of these properties, which represents a measure of the lithospheric resistance to bendind (e.g. Watts and Burov, 2003). Since flexural rigidity depends on the rheology of materials, it is more commonly represented through the effective elastic thickness (T_e), which represents the vertical extent of lithosphere with elastic behavior (e.g. Burov and Diament, 1995; Turcotte and Schubert, 2002; Watts and Burov, 2003; Kirby, 2014). The lithosphere rigidity (D) is related with T_e by means of equation 1 (Watts, 2001; Turcotte and Schubert, 2002)

$$D = \frac{ET_e^3}{12(1-\nu^2)} \tag{1}$$

where E and ν are the Young's modulus and Poisson's ratio, whose standard values are $E = 10^{11}$ Pa, $\nu = 0,25$, respectively (Tassara et al., 2007; Kirby and Swain, 2011, among others). Although the actual lithosphere is constituted by materials of different rheologies, for prolonged periods of time, the deflection produced by the topographic loads could be assessed by considering the lithosphere as an infinite two-dimensional elastic plate overlying a fluid substrate (asthenospheric mantle) (e.g. Burov and Diament, 1995, 1996; Turcotte and Schubert, 2002; Watts, 2001; Watts and Burov, 2003). The flexural response in oceanic and continental lithosphere is different (Watts and Burov, 2003). On the relatively young oceanic lithosphere (which has a single layer rheology), the T_e depends mainly on the thermal age (Watts, 1978). Whereas the older continental lithosphere, generally has many layers with different rheology and hence the lithospheric strength is mainly controlled by: the thermal state (thermo-tectonic age), coupling state of crust-mantle, the crust and mantle thickness mechanically competent, the bending stresses produced by the surface and subsurface loads (for a review see Burov and Diament, 1995). In general, old lithospheres ($> 1.5Gyr$) are stronger ($T_e > 60km$) and colder than weak ($T_e < 30km$) younger lithospheres ($< 1Gyr$) (Pérez-Gussinyé and Watts, 2005; Audet and Bürgmann, 2011). Values from 2 to 50 km of T_e are representative of the oceanic lithosphere Watts and Burov (2003), while T_e values in the continental regions are highly variable. For instance, in old coupled lithosphere the T_e might be higher than $110km$ (Burov and Diament, 1995).

The importance of T_e on orogenic evolution has been recently assessed at a global scale by Mouthereau et al. (2013). According to these authors, the

crustal decoupling depth and the amount of plate shortening during the orogenic building depends on the inherited lithospheric strength. In this sense, young Phanerozoic lithospheres (with a high geothermal gradient) involve deeper crustal deformation and less contraction than strong older lithospheric plates (Mouthereau et al., 2013). Similarly, a study of lithospheric elastic thickness was carried out by Watts et al. (1995) in the Central Andes, as a pioneer work to explain the different deformation styles in the easternmost sector of the Central Andes. These authors proposed that large shortening and thin-skinned deformation style observed in the Subandean system are related to a strong lithosphere represented by high T_e values. Whereas, the thick-skinned deformation and low shortening to north and south of the Subandean system are related to low T_e values. These authors proposed that this variation in T_e, and consequently the deformation styles, were controlled by the proximity to the Precambrian Brazilian craton. These structural contrasts were explained by a simple shear in the Subandean system and pure shear in the Santa Bárbara, which are characterized by a flexural and local (Airy) isostatic mechanisms, respectively (Allmendinger and Gubbels, 1996).

According to most flexural studies in the Central Andes, the lowest T_e values were found along the Andean orogen, increasing the values towards cratonic regions (e.g. Subandean and Santa Bárbara systems), whereas the highest values were found in cratons, far away from the trench (e.g. Stewart and Watts, 1997; Tassara and Yáñez, 2003; Tassara, 2005; Tassara et al., 2007; Pérez-Gussinyé et al., 2008, 2009).

The intermediate to high T_e values estimated to the south of the Subandean system over the Santa Bárbara system (e.g. Stewart and Watts, 1997;

Tassara and Yáñez, 2003; Tassara, 2005; Mantovani et al., 2001, 2005; Wienecke et al., 2007; Pérez-Gussinyé et al., 2009) break the straightforward correlation proposed by (Watts et al., 1995) between the T_e and deformation styles in the Central Andes. Furthermore, for the same region, the T_e values are widely variable from one study to other (e.g. Watts et al., 1995; Stewart and Watts, 1997; Tassara and Yáñez, 2003; Tassara, 2005; Tassara et al., 2007; Mantovani et al., 2001, 2005; Wienecke et al., 2007; Pérez-Gussinyé et al., 2007, 2008, 2009; Kirby and Swain, 2011; McKenzie et al., 2014), showing dependence on the applied methodology (Crosby, 2007; Sacek and Ussami, 2009).

Among the most commonly used methods to estimate T_e are: i) The inverse spectral analysis, by cross-correlating gravity and topography data in frequency domain (e.g. Forsyth, 1985; McKenzie, 2003; Kirby, 2014). In this method, the spatial resolution is enhanced through of techniques as multitaper (e.g. Simons et al., 2003; Pérez-Gussinyé et al., 2009), wavelet (e.g. Kirby and Swain, 2004; Swain and Kirby, 2006; Kirby and Swain, 2011) or convolution (Braitenberg et al., 2002). ii) The gravity forward modeling of the lithosphere and solving the differential equation of a thin elastic plate (e.g. Karner and Watts, 1983; Stewart and Watts, 1997; Turcotte and Schubert, 2002; Wienecke et al., 2007). iii) Analyzing the differences in gravity anomalies between the observed data and the visco-elastic model response (e.g. Mantovani et al., 1999, 2001, 2005)

Sacek and Ussami (2009) have assessed the discrepancy in the T_e values determined in South America through different methododologies (Stewart and Watts, 1997; Tassara et al., 2007; Pérez-Gussinyé et al., 2007). The

authors concluded that the T_e values obtained by forward modelling (Stewart and Watts, 1997) better depict foreland basin depth and gravity anomalies in the Central Andes than T_e values obtained by spectral methods from Tassara et al. (2007); Pérez-Gussinyé et al. (2007). This is because T_e values estimated using spectral methods depend on the window-size. Thus, the T_e is not a simple average value inside a particular window, but the T_e is biased towards lower values (Pérez-Gussinyé et al., 2007; Crosby, 2007). Also, the T_e values calculated by wavelet Bouguer coherence Tassara et al. (2007) are underestimated due to the large-scale of wavelets (Pérez-Gussinyé et al., 2007; Sacek and Ussami, 2009).

In order to better understand the potential relation between the T_e and, style and nature of deformation in the Subandean and Santa Bárbara systems, we elaborate a high-resolution T_e variable map. To achieve this: i) We used a high-resolution gravity dataset from EIGEN-6C4 model (Förste et al., 2014), not used in previous T_e studies in Central Andes. (for instance, Pérez-Gussinyé et al. (2007, 2008, 2009); Tassara et al. (2007) used the EIGEN-CG03C model (Förste et al., 2005), Jekeli et al. (2013) and McKenzie et al. (2014) used data from satellite GOCE (Gravity field and steady-state Ocean Circulation Explorer) (Pavlis et al., 2008, 2012)). ii) We applied a forward modelling method following Sacek and Ussami (2009). iii) We carried out an analysis of the upper mantle-lower crust density values to calculate the gravity Moho that better fits previous seismological data. iv) A study of density values was performed in order to be used the elastic plate model. v) The new methodology applied in this study allowed to calculate the plate deflection by considering all topographic loads in the x-y plane. Then the

T_e value was calculated in a high resolution window. Notably, this is not an iterative method, whereby each T_e chosen is a minimum rms.

2. Tectonic Setting

The Altiplano-Puna Central Andes formed by convergence between South American and Nazca Plates resulted in the largest ($\backsim$ 4 km of elevation) non-collisional mountain chain on the Earth (Silver et al., 1998). As result of a significant crustal shortening since Early-Late Cretaceous, a series of morphostructural provinces were formed (e.g. Sobolev et al., 2006; Barnes and Ehlers, 2009; Carrapa and DeCelles, 2015). Among the main units present in the study area are: Frontal Cordillera (FC), Western Cordillera (WC), Altiplano (AP), Puna (P), Eastern Cordillera (EA), Sierras Pampeanas (SP), Interandean system (IAS), Subandean system (SAS), Santa Bárbara system (SBS) (Figure 1).

We analized two segments of the study region Allmendinger and Gubbels (1996), one to the north of 23°S-24°S in the Altiplano-Subandean system segment, and the other to the south of these latitudes in the Puna-Santa Bárbara system segment.

The northern segment is characterized by a large shortening,a high topography in the Altiplano supported by a thick crust accompanied by a mafic lower crust (Prezzi et al., 2009; Tassara et al., 2006; Tassara and Echaurren, 2012). In contrast, the southern segment presents less shortening and the Puna topographic elevation is similar to the Altiplano but presents a thinner crustal thickness devoid of a mafic lower crust, which might be supported in

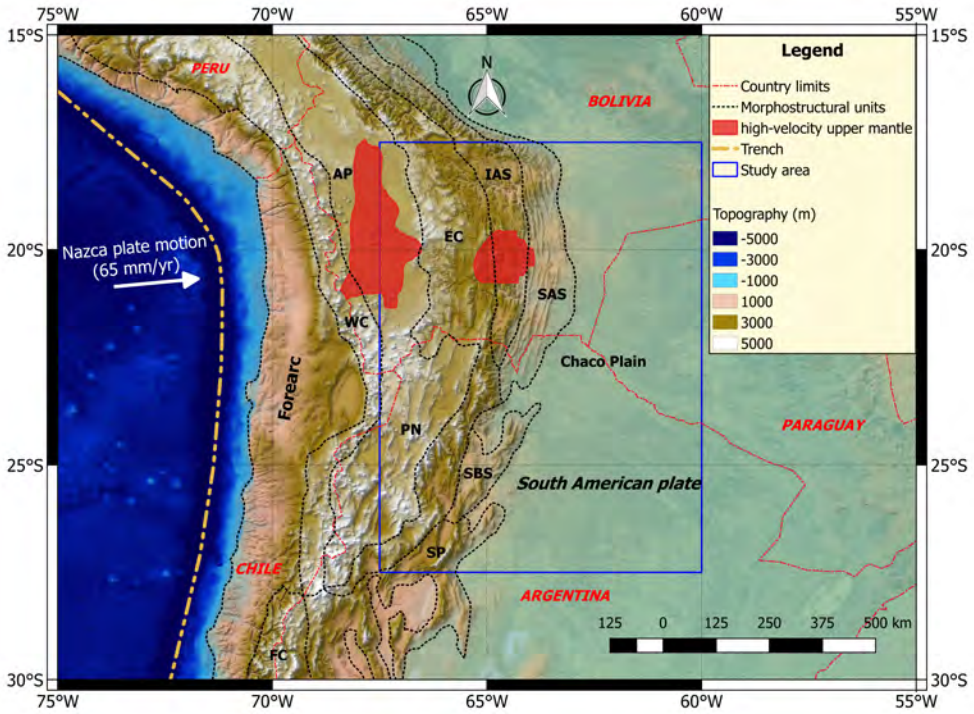

Figure 1: Central Andes orocline over a topography-bathymetry model (Sandwell and Smith, 2009). The main morphostructural units (modified from Barnes and Ehlers (2009); Tassara (2005)) present in the region are: Frontal Cordillera (FC), Western Cordillera (WC), Altiplano (AP), Puna (P), Eastern Cordillera (EA), Sierras Pampeanas (SP), Interandean system (IAS), Subandean system (SAS), Santa Bárbara system (SBS). High-velocities upper mantle zones modified of Myers et al. (1998); Beck and Zandt (2002). Nazca plate motion of Brooks et al. (2011).

part by a shallow asthenosphere (e.g. Yuan et al., 2000, 2002). From gravity forward modeling and using constrains of previous geophysical studied Prezzi et al. (2009); Tassara et al. (2006); Tassara and Echaurren (2012) reported 3D maps of Moho and lithosphere-asthenosphere depths boundaries, which are consistent with these results. In addition, the heat flow in the northern segment differs to the southern (see Figure 5 Hamza et al., 2005). Thus, the highest values of heat flow are observed in the forearc region and in the Western Cordillera ($> 140mW/m^2$). To the east, the heat flow decreases, reaching a minimum value over the Subandean system ($\backsim 40mW/m^2$), increasing towards the distal foreland zone. Whereas, in the southern segment, high heat flow values are found over the Western Cordillera, the Puna, the Eastern Cordillera ($> 140mW/m^2$), the Santa Bárbara system and the proximal foreland ($\backsim 80 - 120mW/m^2$) decreasing toward distal foreland zone (see Figure 9.

Several authors have discussed the main differences in structure and deformation styles of most recent morphostructural units (Allmendinger and Gubbels, 1996; Kley and Monaldi, 1998; Kley et al., 1999), the Subandean system in the northern segment and the Santa Bárbara system in the southern. This two deformation styles were described by (Allmendinger and Gubbels, 1996) and related to simple and pure shear deformation mechanism, respectively. The thin-skinned deformation style of the Subandean system is linked to deformation of a thick Paleozoic sedimentary basin ($> 3km$) distributed extensively into the foreland area over a metamorphic/crystalline basement, unaffected by regional Mesosoic extension (e.g. Allmendinger and Gubbels, 1996; Kley et al., 1999). The deformation in this area was produced

by westward craton underthrusting Eastern Cordillera and part of Altiplano as far as 65.5W (Beck and Zandt, 2002). The latter authors interpreted this lithosperic limit based on different geophysical studies (gravity, seismological, geochemical) (e.g. Dorbath et al., 1993; Watts et al., 1995; Aitcheson et al., 1995; Lamb and Hoke, 1997; Baby et al., 1997; Myers et al., 1998).Kley et al. (1999) observed that the region with high shortening in the Subandean system presents a thick lithospheric mantle and suggested that cratonic lithospheric mantle underthrusting beneath the Central Andes has played an important role in the deformation. Craton subduction and thin-skinned deformation in the Subandean system has been tested and reproduced in numerical modelling studies (Sobolev and Babeyko, 2005; Sobolev et al., 2006). On the other hand, the Santa Bárbara system presents a thick-skinned deformation style which involves less shortening and deeper crustal faulting (10 to 20-24 km of depth) (Comínguez and Ramos, 1995; Cristallini et al., 1997; Kley et al., 1999), linked to inversion of Cretaceous extensional faults belonging to the Grupo Salta rift, reactivated during the Andean contraction (Kley and Monaldi, 1998; Kley et al., 1999; Kley and Monaldi, 2002).

The process of crustal shortening and thickening in the Central Andes could have involve litospheric foundering below the Puna plateau (Kay and Kay, 1993; Kay et al., 1994; Yuan et al., 2000; Beck and Zandt, 2002; Garzione et al., 2006, among many others). Beck and Zandt (2002) assessed this scenario through seismic analysis in the transition of the Altiplano to Eastern Cordillera. They speculated that the mechanism that could have impulsed this lithospheric delamination is a process of density instability induced by eclogitization of mafic lower crust. Later Kay and Coira (2009) dis-

cusss the crustal shortening and lithospheric delamination in the evolution of Altipmalo-Puna Plateau consistent with other processes (change in dip of the subducted plate, crustal melting, deep crustal flow, and shallow ignimbrites eruption). Recently, Beck et al. (2015) based mainly in noise tomography studies postulated two separates zones of delamination with different volcanic patterns suggesting different styles and timing of lithospheric foundering, which might be related to contrasting lithospheric strength (Krystopowicz and Currie, 2013; Beck et al., 2015).

3. Gravity and terrain Data

With the aim to estimate the lithospheric rigidity in the Central Andes we have used: i) a topographic model with resolution of 1' × 1' arc (Sandwell and Smith, 2009) and ii) a high-resolution gravity database obtained from EIGEN-6C4 model (Förste et al., 2014), which combines terrestrial and satellite data. This dataset includes the LAGEOS (LAser GEOdynamics Satellite) GRACE (Gravity Recovery and Climatic Experiment) and the complete dataset from GOCE-SGG (Satellite Gravity Gradiometer) data integrating also terrestrial data (DTU 2'x2' global gravity anomaly grid (Andersen, 2010), EGM2008 (Pavlis et al., 2012)). This model presents a wavelength of maximum resolution $\backsim$ 18 km (degree/order 2190 in spherical harmonics). We have used the classical Bouguer gravity anomaly (AB) (1 mGal = $10^{-5} m/s^2$) obtained by substracting the ellipsoid corrected by gravity effect of the Bouguer plate ($2\pi G\rho_t H$) from gravity on Geoid. Being $\rho_t = 2,67 g/cm^3$, the density of topography; G the universal Newtonian gravitational constant and H the topography in maximum degree/order of

model (Barthelmes, 2009). Then, the topographic correction was applied through algorithms developed by Kane (1962) and Nagy (1966) in the same degree/order of model.

4. Methodology

In the present contribution, the (T_e) was calculated using a Python code developed by Soler (2015) that makes use of open-source libraries Scipy, Matplotlib and Faitando a Terra (Jones et al., 2001; Hunter, 2007; Uieda et al., 2014). In order to achieve this, the next steps were followed: i) Consideration of the flexural model ii) Inversion of the upper mantle-lower crust discontinuity (inverted gravity Moho) iii) Density analysis to be used in the plate model iv) T_e calculation.

4.1. Flexural Model

The lithosphere flexure might be evaluated by considering it as an infinite two-dimensional elastic plate model, as mentioned above (e.g. Turcotte and Schubert, 2002). This model is used when the load is located far from the plate margin (e.g. Watts, 2001). When the load is near to the plate margin, the model used is a broken plate or semi-infinite plate (e.g. Watts, 2001; Turcotte and Schubert, 2002). We used the infinite plate model (Figure 2), as our study area (blue box in Figure 1) is located relatively far away from the margin.

The (Figure 2) shows the regional compensation mechanism (Turcotte and Schubert, 2002). The continental crust with t thickness and density ρ_c

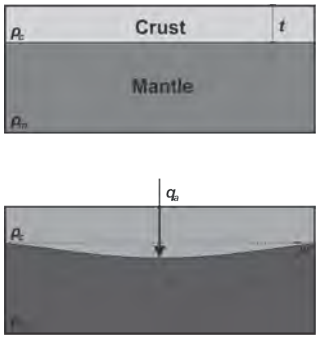

Figure 2: Scheme of regional compensation mechanism (Turcotte and Schubert, 2002). The image above is showing the continental crust separated from upper mantle by the Moho discontinuity, previously to applying the topographic load. The image below, shows the deflection (w) by the applied topographic load q_a, being, t the crust normal thickness, ρ_c the crust density, ρ_m the mantle density

is separated by the Moho discontinuity from upper mantle of density ρ_m. The Moho discontinuity is deflected downward when a load is applied. Thus, the newly created space is filled with crustal rocks (Turcotte and Schubert, 2002). The differential equation 2 (Stewart and Watts, 1997; Garcia et al., 2015) relates the deflection $w(x, y)$ for a known topographic loads $\rho_t g h(x, y)$ distributed in the xy plane, the variable flexural rigidity $D(x, y)$ and the horizontal forces (here equal to zero), as was determined for the study region by Tassara and Yáñez (2003); Tassara (2005).

$$\nabla^2\left[D\nabla^2 w\right] - (1-\nu)\left[\frac{\partial^2 D}{\partial x^2}\frac{\partial^2 w}{\partial y^2} - 2\frac{\partial^2 D}{\partial x \partial y} + \frac{\partial^2 D}{\partial y^2}\frac{\partial^2 w}{\partial x^2}\right] + (\rho_m - \rho_{\text{infill}})gw = \rho_t g h \tag{2}$$

Being ρ_t the topographic density, $g = 9.8 m/s^2$, $h(x, y)$ the topographic elevation and $(\rho_m - \rho_{\text{infill}})gw$ the restoring force, which is equivalent to the force resulting from replacing mantle rocks by crustal rocks in a column

of thickness $w(x, y)$. The last equation is easily solved in the wavenumber ($\mathbf{k} = (k_x, k_y)$) domain by applying the Fourier Transform to each member equation (Brigham, 1974; Watts, 2001). Also, considering D constant, $W(k_x, k_y)$ and $H(k_x, k_y)$ the wavenumber representation of the deflection $w(x, y)$ and topography $h(x, y)$ respectively and using proprieties of Fourier Transform, the deflection is determined by the following equation 3 (Watts, 2001).

$$W(k_x, k_y) = \frac{\rho_t}{\rho_m - \rho_{\text{infill}}} \Phi_e(k) H(k_x, k_y) \tag{3}$$

Where the function $\Phi_e(k)$ is given by the equation 4:

$$\Phi_e(k) = \left[\frac{Dk^4}{(\rho_m - \rho_{\text{infill}})g} + 1 \right]^{-1} \tag{4}$$

4.2. Gravity Moho Inversion

The gravity Moho depths were determined from the inversion of gravity anomalies (AB). This was obtained by adding the normal crustal thickness t to the inverted deflection w_{inv}, which was calculated using the Parker-Oldenburg algorithm (Parker, 1973; Oldenburg, 1974). This was computed by an iterative method through equation 5 which starts with an arbitrary deflection (w_0) and iterate until a desired error is reached.

$$\mathcal{F}\Big[w_i\Big] = -\frac{\mathcal{F}\big[AB\big]e^{kt}}{2\pi G(\rho_m - \rho_c)} + \sum_{n=2}^{N} \frac{(-1)^n k^{n-1}}{n!} \mathcal{F}\Big[w_{i-1}^n\Big] \tag{5}$$

The previous equation consists in calculating the deflection (w_i) from the one obtained in the previous iteration (w_{i-1}). Being $\mathcal{F}$ the Fourier trans-

form, AB the Bouguer anomaly, t the normal crustal thickness, G the Universal gravitational constant, ρ_m the upper mantle density, ρ_c the lower crust density, N, maximum summation order (In this work the desired error was reached with order equal to 18), n index of summation and k the wave-vector module.

The first term of the equation 5 amplifies the high-frequencies, so the algorithm convergence is achieved using a low-pass filter (e.g. Oldenburg, 1974; Braitenberg and Zadro, 1999; Gómez-Ortiz and Agarwal, 2005). The Hamming filter was applied on each iteration following Soler (2015).

$$\text{Hamming Filter} = \begin{cases} \frac{1}{2}[1 + cos(\pi \frac{k}{k_{cut}})] & k < k_{cut} \\ 0 & k \geq k_{cut} \end{cases} \tag{6}$$

Considering a cutoff wavenumber ($k_{cut} \backsim 0.0538$) equivalent to a wavelength of $\lambda \backsim 116$ km, which according to the equation 7 proposed by Featherstone (1997):

$$z = \frac{R\lambda}{(360 - \lambda)} \tag{7}$$

corresponds to mass anomalies at a depth of $\backsim 18$ km, where R is the mean Earth radius. Since our objective is to determine the upper mantle-lower crust discontinuity (gravity Moho) depth, equivalent frequencies of mass of upper crust shallower than $\backsim 18$ km were eliminated.

In order to estimate the gravity Moho, a normal crustal thickness of 35 km (e.g. Assumpção et al., 2013; Prezzi et al., 2014) and a mean density contrast between upper mantle and lower curst ($\rho_m - \rho_{lc}$) equal to $0.41 g/cm^3$

	P-wave velocity (V_p [km/s])	Density [g/cm^3]
Topography		ρ_t =2.67
Foreland sediment	2.80	ρ_f =2.25
Arbitrary sediment		ρ_s =2.40
Upper crust	6.35	ρ_{uc} =2.69
Lower crust		ρ_{lc} =2.89
Upper mantle	8.05	ρ_m =3.30

Table 1: Velocities and it respective densities used

were considered (Figure 3, up-left). To obtain these values, we converted mean P-wave velocities of the study area from maps reported by Chulick et al. (2013) in density values using the equation of Brocher (2005) (see table 1). The density values obtained for the upper crust, lower crust, and upper mantle (ρ_{uc}, ρ_{lc}, ρ_m) were $2.69g/cm^3$, $2.89g/cm^3$ and $3.30g/cm^3$, respectively. In comparison, similar density contrast values ($0.40g/cm^3$) have been considered by others authors (Tassara, 2005; Uieda and Barbosa, 2017) to estimate the Moho depth from gravity data in the Central Andes. Other lithospheric density values have been estimated and used by Tassara et al. (2006) and Prezzi et al. (2009) in three-dimensional forward gravity model considering a set of 3D bodies. The upper mantle value used by these authors is comparable with the ones used in this work, while the lower crust density is lower than the one used in this work, implying in our model of two layers a lower upper mantle-lower crust density contrast. Thus, the gravity Moho depth was calculated by considering a density contrast value equal to $0.30g/cm^3$ and $0.22g/cm^3$ (Figure 3, up) by following Tassara et al. (2006) and Prezzi et al. (2009), respectively.

With the aim to choose the right density contrast value and, consequently, the adequate inverted Moho to be used in the computation of the (T_e), the

	Moho from Assumpção et al. (2013)			
	Mean	standard deviation	minimum	maximum
Inverted Moho ($\Delta\rho$ =0.41)	1.11	3.36	-14.73	14.33
Inverted Moho ($\Delta\rho$ =0.30)	4.2	5.38	-6.97	25.01
Inverted Moho ($\Delta\rho$ =0.22)	8.41	9.24	-5.66	42.31

Table 2: Statistical analysis of the differences between Moho from gravity using different density contrasts of upper mantle - lower crust ($\Delta\rho$) mentioned above and the Moho from (Assumpção et al., 2013).

differences between each inverted Moho (Figure 3, up) and the recently Moho published by Assumpção et al. (2013) for South America using seismological methods, were estimated. A statistical analysis of these differences was made. The histograms, average, standard deviation, minimum and maximum values corresponding to these differences are shown in Figure (3, down) and in the Table 2. This comparison shows that the inverted Moho obtained using a density contrast (upper mantle density — lower crust) equal to $0.41 g/cm^3$ is the one that best correlates with the seismological Moho depth from Assumpção et al. (2013). In the same way, the difference and the statistical analysis between obtained inverted Moho and recent gravity Moho determined by Tassara and Echaurren (2012) and Uieda and Barbosa (2017), as well as, seismological Moho from (Assumpção et al., 2013) were also calculated. These results are shown in Figure (4).

4.3. Densities Analysis

Calculation of deflection (w) through equation 3 requires to know the densities of rocks that fill the void space (ρ_{infill}) deflected downward, the topography (ρ_t) and upper mantle (ρ_m). In order to choose the right value to be used in the model, different average crustal densities were considered.

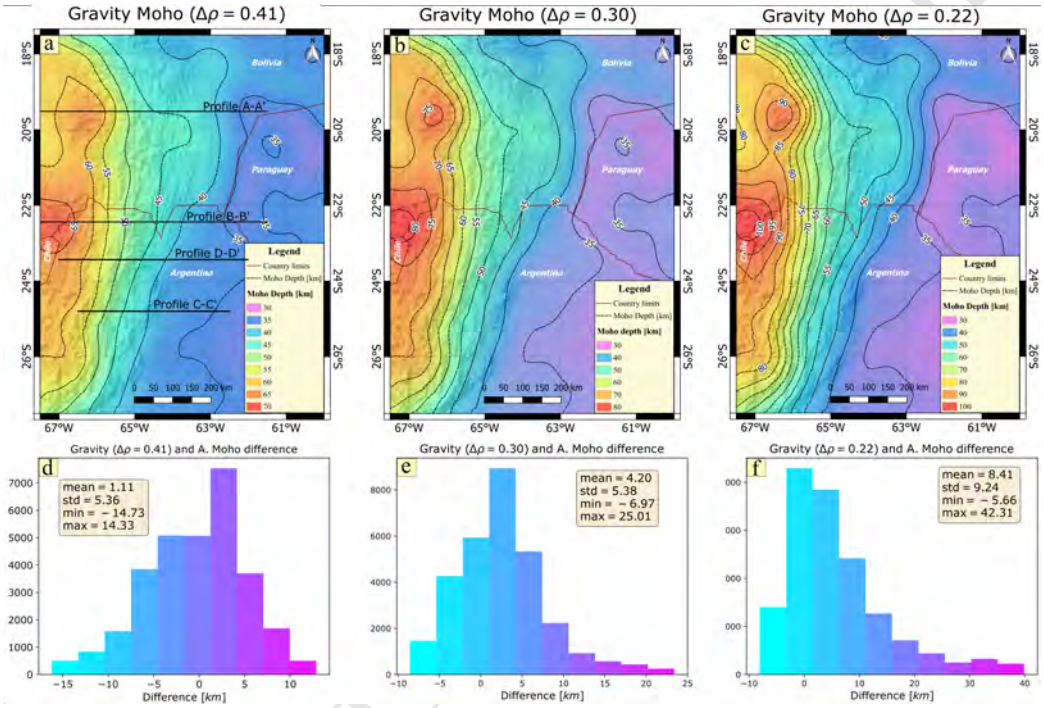

Figure 3: Up) Gravity Moho discontinuity inverted from the gravity anomalies using different density contrasts of upper mantle-lower crust ($\rho_m - \rho_l c$), a) $0.41 g/cm^3$, b) $0.30 g/cm^3$ and c) $0.22 g/cm^3$. Down) Histograms of the difference between seimological Moho from Assumpção et al. (2013) (A) and gravity inverted Moho using a contrast ($\rho_m - \rho_l c$) of $0.41 g/cm^3$ (d), $0.30 g/cm^3$ (e) and $0.22 g/cm^3$ (f). Being; mean, std, min and max; the average, standard deviation, minimum and maximum respectively. Straight lines shows the location profiles over the Subandean system (A-A'), Santa Bárbara system (C-C'), (B-B') and (D-D') intermediate profiles.

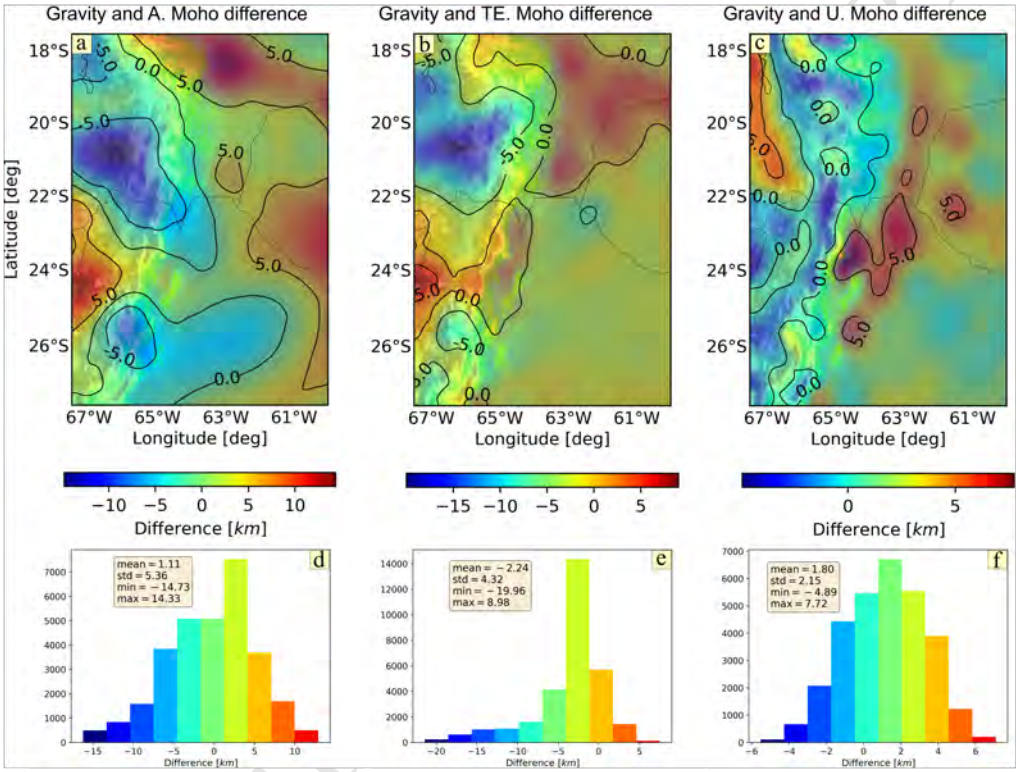

Figure 4: Difference between gravity Moho (using a density contrast ($\rho_m - \rho_l c$) of $0.41 g/cm^3$) and Moho obtained by, a) Assumpção et al. (2013) (A), b) Tassara and Echaurren (2012) (TE), c) Uieda and Barbosa (2017) (U). Being; mean, std, min and max; the average, standard deviation, minimum and maximum respectively.

Each density value generates a specific deflection produced by the load. The used densities were: foreland sediment (ρ_f), arbitrary sediment (ρ_s), upper crust (ρ_{uc}) and lower crust (ρ_{lc}) (see values in Table 1). The average density of foreland sediments was obtained from seismic velocities reported by Comínguez and Ramos (1995) using equation of Gardner et al. (1974). Similar values of foreland sediments have been used by Prezzi et al. (2014). The upper and lower crust density values were specified previously. The arbitrary sediment infill density was considered using a global mean value between foreland sediments and upper crust. Prezzi et al. (2009) have calculated a similar density values for the Chaco basin; and equal sediment density values have been used in others regional flexural studies (e.g. Arnaiz-Rodríguez and Audemard, 2014). Every deflection and their gravity anomalies were calculated using as infill density the values of crustal density above mentioned (i.e., ρ_f, ρ_s, ρ_{uc} and ρ_{lc}). For each density, a series of hypothetical values of T_e were considered ranging from 0 to 100 km and by using the equations 3 and 4, deflections (w_i) to each value of T_e were calculated. Then, gravity effect of every deflection (w_i) was calculated by approaching through rectangular prisms. This was carried out by using the functions in fatiando.gravmag of Fatiando a Terra (Uieda et al., 2014).

On the other hand, the high frequencies present in gravity Bouguer anomaly (AB) were filtered to estimate a regional gravity anomaly. This regional anomaly was obtained following a method proposed by Pacino and Introcaso (1987). In this sense, first the inverted gravity Moho was calculated and then, its gravimetric effect was computed using the functions mentioned above (Uieda et al., 2014). Also, the regional anomalies were calculated

through the classical upward continuation method (Jacobsen, 1987; Blakely, 1995) to $20km$, $25km$ and $30km$. In this way, we observed that the regional anomalies obtained by different methods are consistent. Then, these data was plotted along two profiles (Figures 5 and 6), one across to Subandean system (A-A') and another in the Santa Bárbara system (C-C') (see location in Figure 3).

The foreland basin system is controlled mainly by flexural subsidence related to the topographic load (Jordan, 1981; DeCelles y Giles, 1996). For a geological interpretation, a more reliable approach is to determine the (T_e) by comparing the subsidence predicted by the elastic plate model with the foreland basin depth (e.g. Sacek and Ussami, 2009). In this sense, to estimate the (T_e) from other analysis, we compared the calculated deflections (using ρ_f, ρ_s, ρ_{uc} and ρ_{lc}) with the foreland Chaco basin depth (Figure 7). The foreland sediment depth was obtained from a seismic line with NW-SE strike published by Bianucci (1999); Comínguez and Ramos (1995), which crosses the profile B-B' (see location in Figure 3). These authors identified the basement depth of the Chaco basin in time domain. Then, using the P-wave velocity reported by such authors, we obtained the foreland depth in the intersection ($z_f \backsim 2.1$ km) between the seismic line (s) and the profile (B-B') (Figure 7). Similarly, the profile D-D' crosses two seismic line (s1 and s2) ((Bianucci, 1999; Comínguez and Ramos, 1995). In this case the analysis was carried out for extreme values (ρ_f and ρ_{lc}). The foreland depths were obtained in the same way than in profile B-B' (Figures 8). Foreland depths of $z_f1 \backsim 2.7$ km and $z_f2 \backsim 4.34$ km) were found in the intersection between the seismic lines and our profile (D-D').

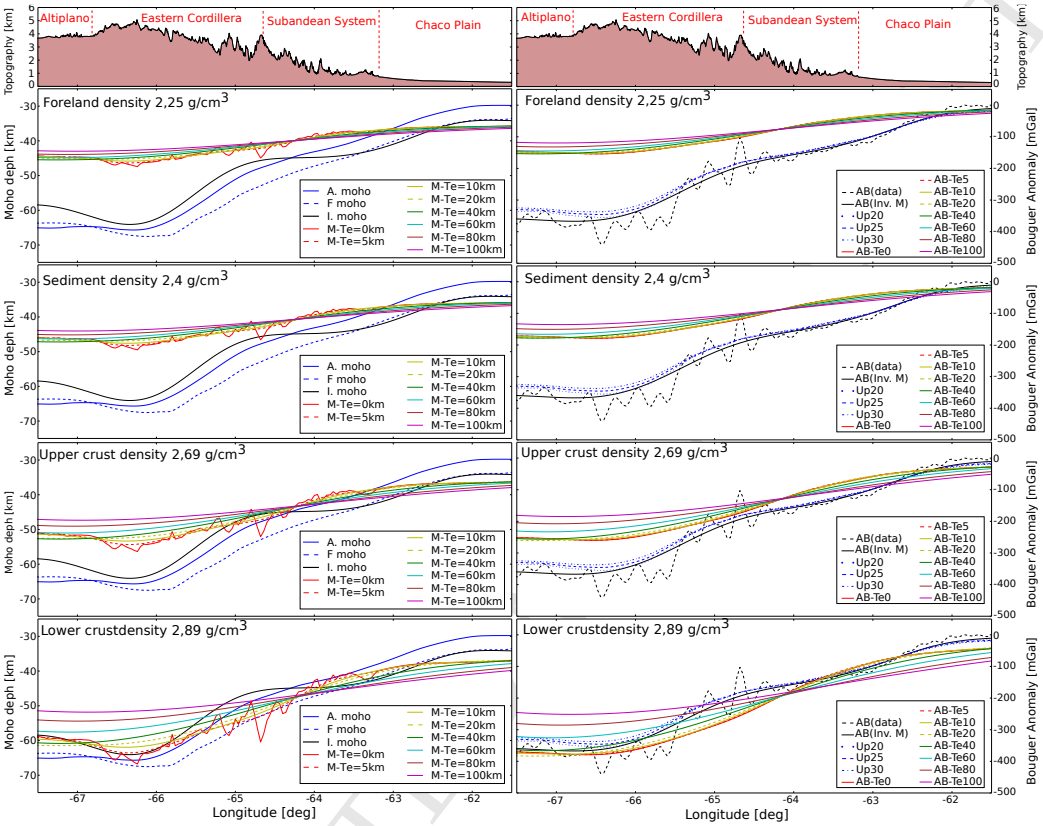

Figure 5: Profile across the Subandean system (A-A') (see location in Figure 3). Left plot shows the comparison between: our gravity Moho (I. Moho), regionals seismological Moho (Assumpção et al. (2013) (A. Moho), Feng et al. (2007) (F. Moho)), and plate deflections (using T_e form 0 to 100 km). This comparison is carried out considering different infill density values of crust rocks (foreland sediment (ρ_f), arbitrary sediment (ρ_s), upper crust (ρ_{uc}) and lower crust (ρ_{lc}) densities). Right plot shows the comparison between: the gravity effects of all plate deflections and the regionals anomalies: upward continuation the Bouguer anomaly (AB data) to $20km$, $25km$, $30km$ (Up20, Up25,Up30, respectively) and the gravimetric effect of inverted Moho (AB(Inv. M)). Topography (Shuttle Radar Topography Mission (SRTM 90m))

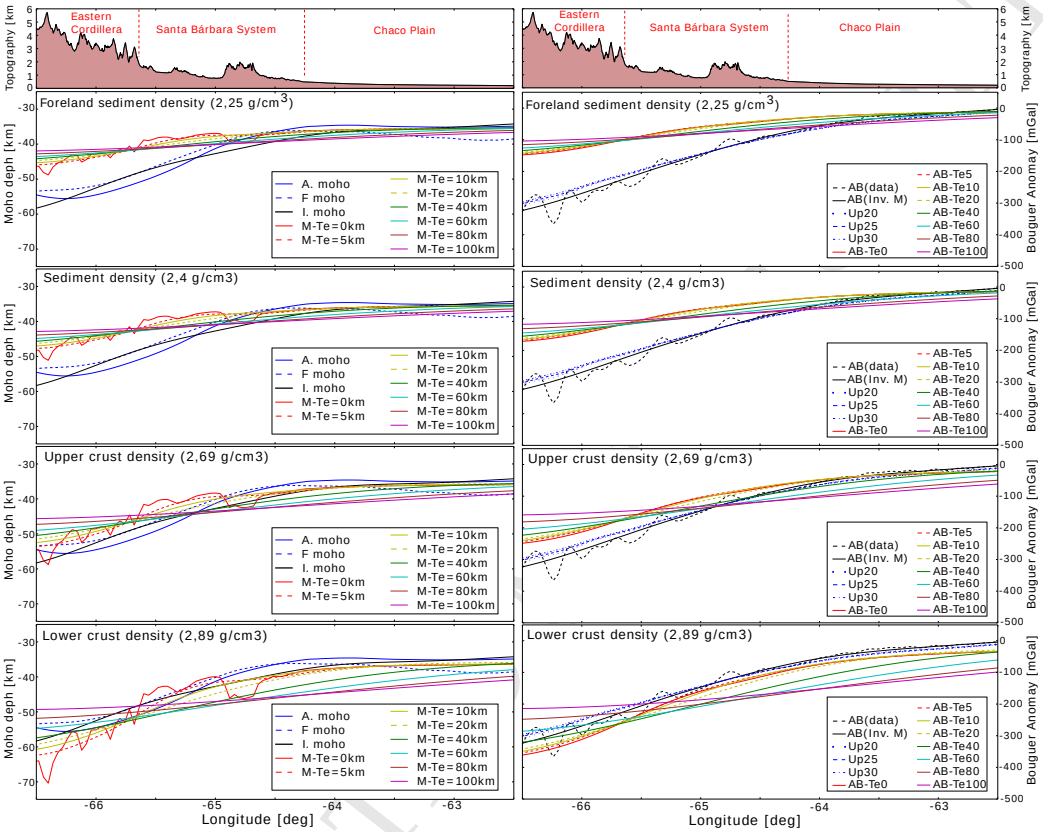

Figure 6: Profile Santa Bárbara system (C-C') (see location in Figure 3). Left plot shows the comparison between: our gravity Moho (I. Moho), regionals sesmological Moho (Assumpção et al. (2013) (A. Moho), Feng et al. (2007) (F. Moho)), and plate deflections (using T_e form 0 to 100 km). This comparison is carried out considering different infill density values of crust rocks (foreland sediment (ρ_f), arbitrary sediment (ρ_s), upper crust (ρ_{uc}) and lower crust (ρ_{lc}) densities). Right plot shows the comparison of gravity effect af all plate deflections and the regionals anomalies from upward continuation the Bouguer anomaly (AB data) to $20km$, $25km$, $30km$ (Up20, Up25,Up30, respectively) and the gravimetric effect of inverted Moho (AB(Inv. M)). Topography (SRTM 90m)

4.4. Estimation of Effective Elastic Thickness

From the analysis of deflections using different infill densities, we observed that the deflection of plate model calculated by considering a lower crust rocks density as infill best predicts the Moho in Central Andes and foreland Chaco basin depths. Likewise, the gravity anomaly of this model also predicts the gravity Bouguer anomaly in Central Andes. For this reason this density value was chosen and used in equation 3 to obtain the T_e map (Figure 9). The code Soler (2015) implemented in this work contains an interface which allows choosing windows with variables positions and sizes. We used windows of 100 $\times$ 100 km. For every specific window, several hypothetical values of T_e were used and their respective deflections (w_i) were obtained by considering the topography load for the whole study area through the equation 3. Then, every w_i is compared with the inverted gravity deflection w_{inv} and the T_e that presents the minimum rms (root-mean-square) value between both deflections will be assigned to the center of the window. By performing this step on several windows all over the study area, we obtain the maps with variable T_e and rms (Figures 9 and 10). Noteworthy, this code allows to choose a window that presents a unique solution, identified as a minimum rms.

5. Results

The gravity inverted Moho (Figure 3) was calculated using different lower crust- upper mantle density contrasts ($0.41 g/cm^3$, $0.30 g/cm^3$ and $0.22 g/cm^3$). The first value was obtained from mean of P-wave velocities maps of the study

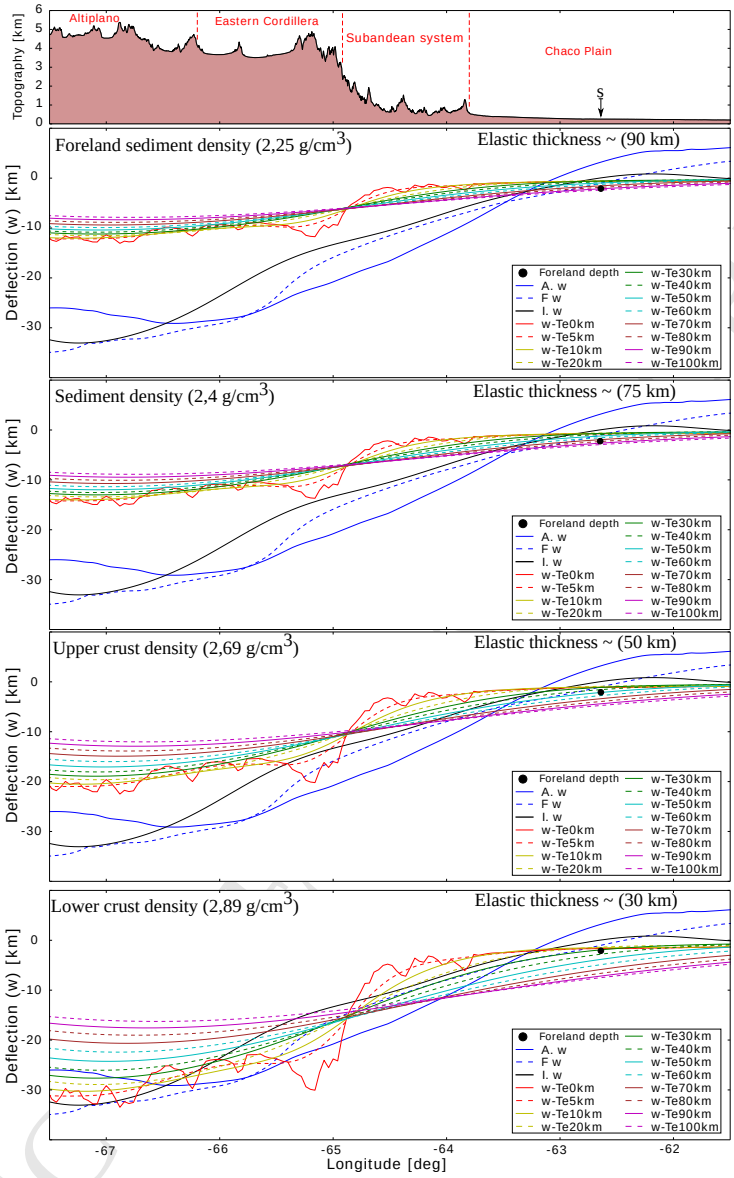

Figure 7: Profile B-B' (see location in Figure 3). Comparison between plate deflections (w) (using T_e form 0 to 100 km), foreland sediment depth obtained from a seismic line (s) (Bianucci, 1999; Comínguez and Ramos, 1995) that crosses this profile, the gravity inverted deflection (I.w) and the seismological Moho less normal thickness from Assumpção et al. (2013) (A.w) and Feng et al. (2007) (F.w). This comparison was carried out considering different infill density values of crustal rocks (foreland sediment (ρ_f), arbitrary sediment (ρ_s), upper crust (ρ_{uc}) and lower crust (ρ_{lc}) densities). Topography (SRTM 90m)

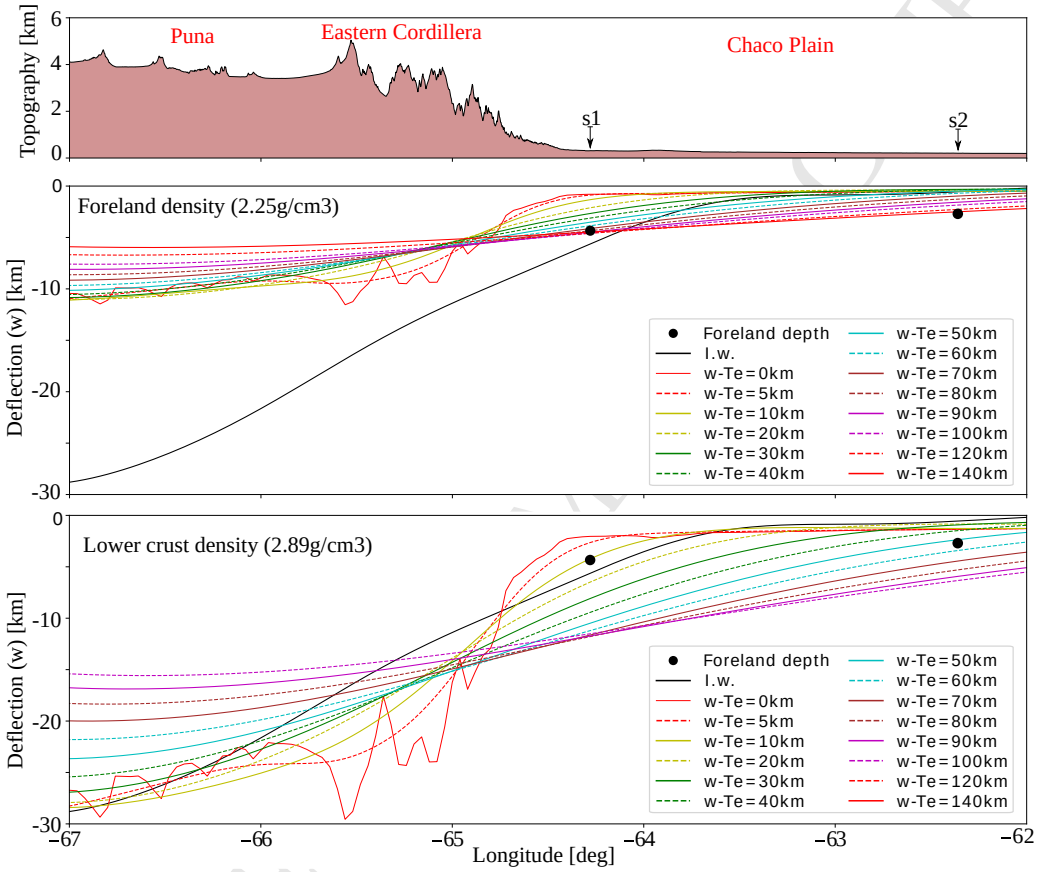

Figure 8: Profile D-D' (see location in Figure 3). Comparison between plate deflections (w) (using T_e form 0 to 100 km), foreland sediment depths obtained from a seismic lines (s1 and s2) (Bianucci, 1999; Comínguez and Ramos, 1995) that crosses this profile. This comparison was carried out considering foreland sediment (ρ_f) and lower crust (ρ_{lc}) densities). Topography (SRTM 90m)

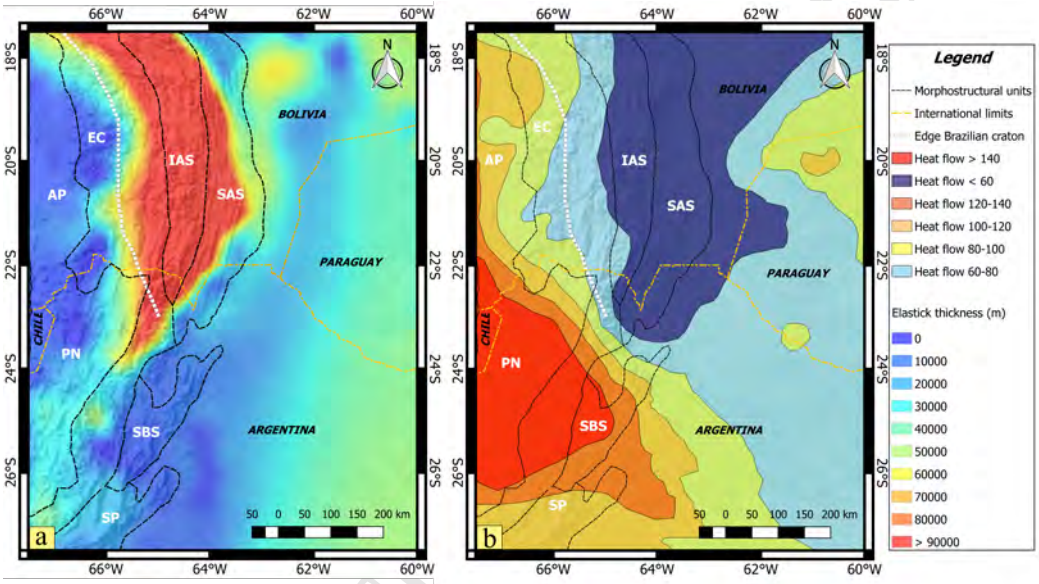

Figure 9: a)Effective elastic thickness (T_e) map. b) Heat flow map modified of Hamza et al. (2005). The Altiplano (AP), Puna (P), Eastern Cordillera (EA), Sierras Pampeanas (SP), Interandean system (IAS), Subandean system (SAS) and Santa Bárbara system (SBS) are the main morphostructural units of the Central Andes (modified of Barnes and Ehlers (2009); Tassara (2005)). Brazilian shield limit from Beck and Zandt (2002).

area (Chulick et al., 2013). The other two were calculated using density values from Prezzi et al. (2009) and Tassara et al. (2006), respectively. From this comparison we observed that the Moho depth in Central Andes is deeper as the density contrast is lower, exceeding the $65km$ $80km$ and $100km$ for the densities mentioned above, respectively. A comparison of these gravity Moho with the seismological Moho from Assumpção et al. (2013) shows that the inverted gravity Moho using a contrast of $0.41g/cm^3$ fits better the seismological Moho, being the mean difference between both equal to $1.11km$ (see Figure 3 (d) and table 2). For the density contrast of $0.3g/cm^3$ and $0.22g/cm^3$, the error is higher, reaching values of $4.2km$ and $8.41km$, respectively. From this statistical analysis the gravity Moho depth calculated with a contrast of $0.41g/cm^3$ was chosen. The difference between the gravity Moho and regionial seismological Moho from (Assumpção et al., 2013) is shown in Figure (4, a and d). Also, we compared with the gravity Moho from Tassara and Echaurren (2012) and the more recently published gravity Moho values for South-America by Uieda and Barbosa (2017). The mean differences between these gravity Moho and our results are relatively low, presenting a better correlation with the Moho from Uieda and Barbosa (2017), which is based on a newer and higher resolution database. These good correlation with above mentioned works (Figure 4) is not only supporting the density contrast chosen, but also the normal crustal thickness used in this study to estimate the gravity Moho. In addition, a comparison between the chosen gravity Moho and the seismological Moho from (Feng et al., 2007) and (Assumpção et al., 2013) was made across two transversal profiles along the Andes, one located in Subandean system (profile A-A') and another Santa

Bárbara (profile C-C') (Figures 5 and 6). Below the Altiplano, values of gravity Moho depth above 60 km are found. These values decrease towards east reaching 50 km. Over the Subandean and Santa Bárbara systems the depth values are less than 40 km. Towards the Chaco plain, the gravity Moho depth reaches shallower values of about 35 km (Figure 3 (a)).

From the analysis of the density values of the plate model, we observed that the deflections calculated considering a lower crust density value as infill density (ρ_{infill}) better predict the gravity or seismological Moho in Central Andes (Figures 5 a and 6 a). Whereas every deflections calculated using a lower infill density (ρ_f, ρ_s, ρ_{uc}), for T_e values ranging from $0km$ to $100km$ underestimate the Moho depth (Figures 5 and 6.

The comparison between plate deflections and the foreland basin depths shows that the T_e values have a strong dependence on the density value used in the plate model (Figure 7). In case of the profile B-B', T_e values of 90 km, 75 km, 50 km and 30 km were found corresponding to each density value ρ_f, ρ_s, ρ_{uc} and ρ_{lc}, respectively. Unlike the previous profile (B-B'), the profile D-D'(Figure 8) contains foreland depth obtained from two seismic lines (Comínguez and Ramos, 1995; Bianucci, 1999), one crossing nearby to the deformation front (s1) and the other crossing far from the latter area (s2) allowing to observe longitudinal variations in foreland depth (Figure 8). In this profile the deflections calculated considering the foreland sediment density, resulting in T_e values of 80 km and higher than $140km$ for s1 and s2, respectively. Whereas, using a lower crust density value, the foreland depth implicated T_e values of $10km$ and $50km$ for s1 and s2. Thus, we observed that the plate deflections calculated considering the lower crust

density better predict the foreland basin depth, while the lower density values underestimate deflections and, in consequence, overestimate the T_e values. This underestimated deflections are the result of a high density contrast in equation 3. The deflections obtained using a density contrast between upper mantle and lower crust of $0.41 g/cm^3$ effectively predict the Moho and foreland depths.

The mean rms of $\backsim$ 1.18 km implicate that all values of T_e determined have low errors. In the Santa Bárbara and Subandean systems, which are the main target of this study, we obtained rms values less than $\backsim$ 1 km. T_e values lower than 10 km were found in the Santa Bárbara system. Low values were also found in the western sector of the Eastern Cordillera, the Puna and Altiplano regions (Figure 9). In Chaco plain the (T_e) progressively increases eastwards reaching values over 50 km. On the other hand, high values of T_e were observed in the easternmost sector of the Eastern Cordillera and over the Subandean system (Figure 9). It is worth to note that these high T_e values have a strong correlation with the Brazilian craton boundary and with the orogenic curvature (Figure 9).

Notably, the highest T_e values (greater than 90 km) observed in profile A-A' between 66° - 63° W are spatially correlated with a shallow zone in the determined inverted gravity Moho (Figure 5 a, black line). This shallow area is the result of a local high-gravity anomaly, which was identified in the regional Bouguer anomalies (Upward continuation and gravity Moho effect). Noteworthy, a similar shallow Moho zone is observed in the Moho derived from receiver function at $\backsim$ 20°S by (Yuan et al., 2000, see Figure 3). Additionally, it is coincident with the high-velocity zone in upper mantle identified

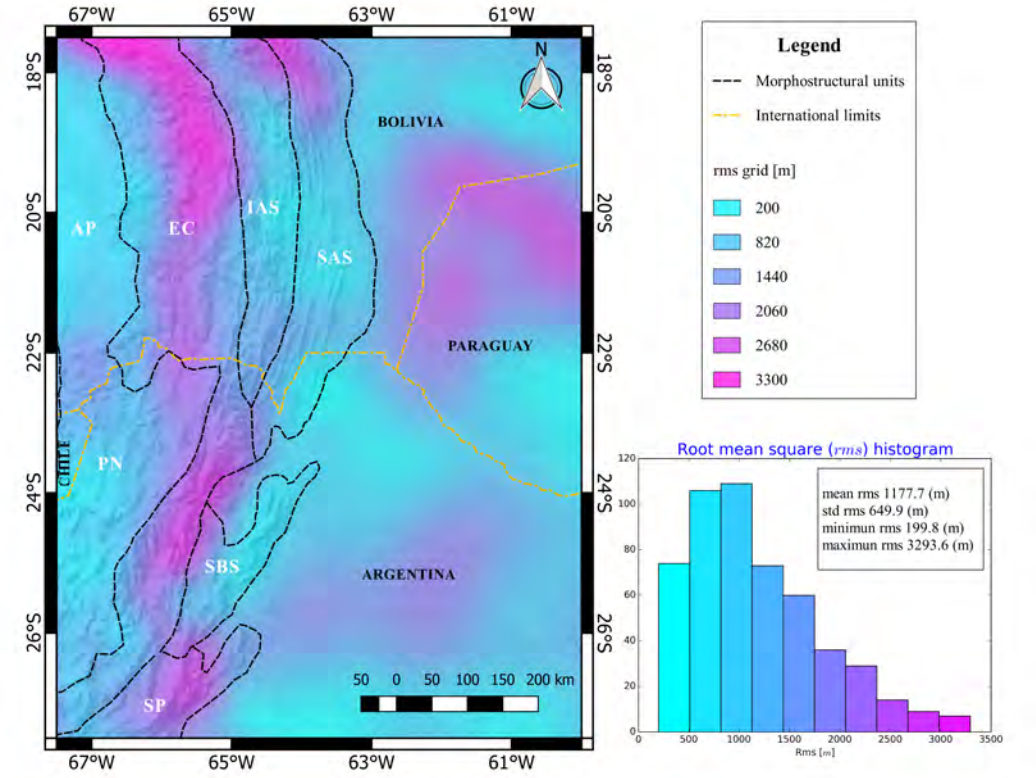

Figure 10: Root mean square (rms) between gravity inverted and plate deflection model. Altiplano (AP), Puna (P), Eastern Cordillera (EA), Sierras Pampeanas (SP), Interandean system (IAS), Subandean system (SAS) and Santa Bárbara system (SBS) are the morphostructural units (modified of Barnes and Ehlers (2009); Tassara (2005))

through seismilogical data by Myers et al. (1998) between 66° - 63° W (red boxed in Figure 1). Moreover Wigger et al. (1994) at 16°S determined a high-velocity zone of lower crust extending from the limits Altiplano-Eastern cordillera to under Subandean system using seismic refraction studies.

Finally, this correlation found between the shallow zone in the gravity Moho (or its gravity effect) and high T_e values is shown over 8 parallel profiles (P1 to P8), from north to south (See Figure 11 a). To better highlight the shallow Moho zone we elaborated a residual anomaly (Figure 11 b) by subtracting a lineal trend (yellow dashed line, Figure 11 a). The obtained residual anomaly evidences that the high-density zone linked to the shallow gravity Moho is present along the Subandean system and the easternmost sector of the Eastern Cordillera (Figure 11).

6. Discussion and Conclusion

The simple correlation between deformation styles in the easternmost sector of the Central Andes and the T_e proposed by Watts et al. (1995) has been weakened by subsequent studies presenting contrasting T_e results (e.g Sacek and Ussami, 2009, among others mentioned above). In order to solve this issue, we applied a forward method as was suggested by Sacek and Ussami (2009) using a high-resolution gravity dataset (Förste et al., 2014).

Our T_e map (Figure 9) shows strong lateral variations from the Andean region to the Chaco plain in the foreland region. Notably, over the morphostructural units in the easternmost sector of the Central Andes, the T_e determined in this contribution shows an striking correlation with deforma-

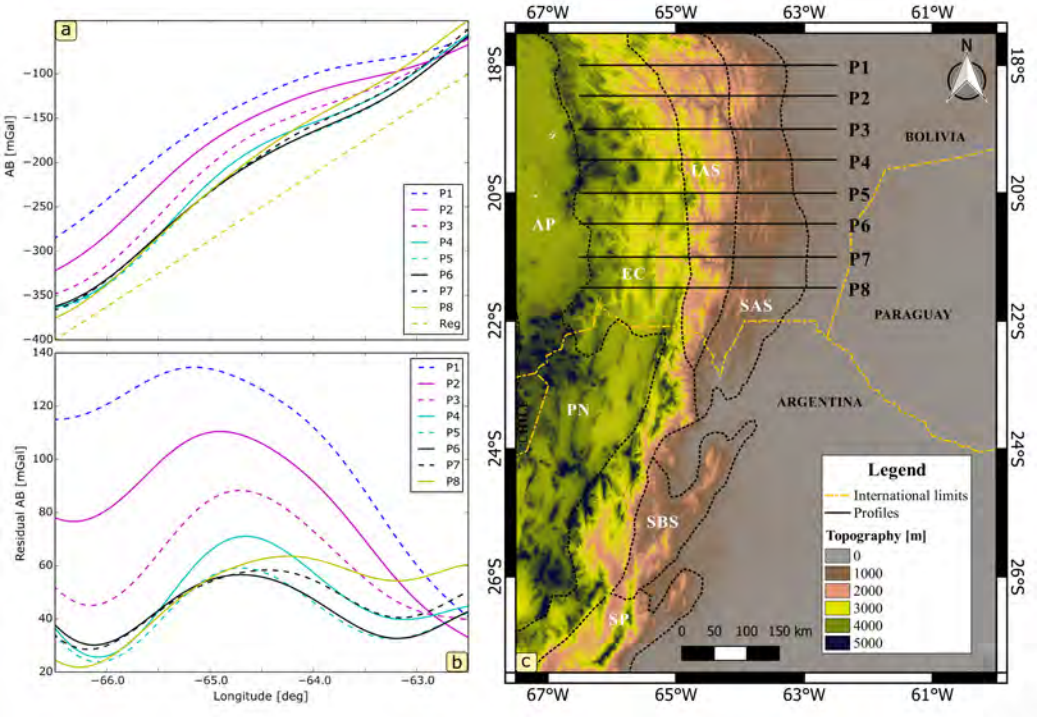

Figure 11: Parallel profiles (P1 to P8) from north to south (location in c) crosses the Subandean system. a) Moho gravity effect showing shallow zone over all profiles. Being the yellow dashed line, the lineal trend (Reg.). b) Residual anomalies profiles obtained by subtracting a lineal trend (Reg.). Altiplano (AP), Puna (P), Eastern Cordillera (EA), Sierras Pampeanas (SP), Interandean system (IAS), Subandean system (SAS) and Santa Bárbara system (SBS) are the morphostructural units (modified of Barnes and Ehlers (2009); Tassara (2005)). Topography (SRTM 90m).

tion styles and mechanisms as previously suggested by Watts et al. (1995). In this sense, the lowest T_e ($\backsim$ 10 km) is found over the Santa Bárbara system where thick-skinned tectonics and pure-shear mechanics have been proposed (Allmendinger and Gubbels, 1996; Kley and Monaldi, 1998). On the other hand, highest T_e values are found mainly over the thin-skinned Subandean system and the easternmost edge of the Eastern Cordillera, where a simple-shear mechanism of deformation has been proposed in relation to craton understhrusting (Beck and Zandt, 2002; Baby et al., 1997; Lamb and Hoke, 1997). We note that this area of highest T_e values is correlated with the orogenic curvature and the western boundary of the underthrusted Brazilian craton (Figure 9).

A comparison T_e results obtained in this study with other flexural studies (Tassara and Yáñez, 2003; Watts et al., 1995; Stewart and Watts, 1997; Mantovani et al., 2001, 2005; Tassara, 2005; Tassara et al., 2007; Pérez-Gussinyé et al., 2009), shows that: i) The precise correlation between the lowest T_e values and the entire Santa Bárbara system, and the highest T_e values over Subandean system and part of Eastern Cordillera are not observed in previous works. ii) Contrary, to most works showing an homogeneously high T_e over the Chaco plain, our results show important lateral variations in this area, from low to intermediate values near the orogenic front to high values towards the cratonic region.

Noteworthy, an inverse correlation between the T_e values obtained in the present contribution and the heat flow map determinate by (Hamza et al., 2005) for the Central Andes is observed (Figure 9. In this sense, the highest T_e values observed over Subandean system and eastern extreme of the Eastern

Cordillera are correlated with very low heat flow. In adition, the low T_e values observed in the Puna, the Altiplano and the Santa Barbara system are correlated with high heat flow. Also, lateral variations in T_e observed in the Chaco plain, correlate with heterogeneous heat flow values in the cratonic region. Therefore, the lithospheric strength in the Central Andes seems to be controlled by the lithospheric thermal state as was suggested by Burov and Diament (1995). A similar inverse correlation has been observed by others works, for example, Tassara (2005) in north segment of the Central Andes (Altiplano-Subandean system), (Sánchez et al., 2017, this issue) in Chilean-Pampean flat-slab, Deng et al. (2014) in south China, among others.

We observed that the highest T_e values (above 90 km) are the result of a shallower zone in the gravity Moho (Figure 5). This shallow zone breaks the long trend of deflection observed in the Central Andes, therefore very high T_e values are required in the plate model in order to adjust the deflection to the shallow Moho zone. A major question is regarding to the origin of the shallow Moho zone. A possibility is that this region could be the result of a local high-gravity anomaly observed in regional anomalies (Figures 5 and 11). This area correlates with a high-velocity lithospheric anomaly reported by Myers et al. (1998) (red box, in Figure 1). Moreover, it is also consistent with seismological studies in this area (Wigger et al., 1994; Yuan et al., 2000).

Large orogenic thickening and upper plate shortening in this sector of the Central Andes are a favorable environment for the formation of lower crustal high-density rocks (Kay and Kay, 1993; Kay et al., 1994; Yuan et al., 2000; Beck and Zandt, 2002; Sobolev and Babeyko, 2005; Sobolev et al., 2006; Babeyko et al., 2006; Garzione et al., 2006, among others). Where

crustal depths greater than 45-50 km are achieved, such as in the analyzed local shallow gravity Moho region, petrological changes take place in the lower crust due to deep rock transformation into high-pressure eclogite (e.g Dewey et al., 1993; Beck and Zandt, 2002). Notably, the presence of such metamorphic facies may cause a depth difference in the Geophysical and Petrological Moho. The latter is identified as a compositional change (felsic-mafic to ultramafic rock composition in peridotite), while the geophysical discontinuity is characterized by changes in density and the elastic properties (Mengel and Kern, 1992; Giese et al., 1999). In this sense, it could be thought that the shallow local gravity Moho could be indicating the presence of high-density rocks (eclogite) in the crust-mantle transition producing a shallower geophysical Moho. This interpretation is consistent with the observations of Giese et al. (1999), who proposed a shallower geophysical Moho respect to the petrological one in Eastern Cordillera explained by the presence of eclogite facies in the lower crust. In this sense, the anomalous zone of very high T_e values may not be entirely related to an elastic lithosphere, but instead it could be a consequence of the presence of high-density rocks in the lowermost crust and related to shallower geophysical Moho.

Acknowledgements

We appreciate Dr. Federico Dávila and anonymous reviewer for their constructive comments and suggestions that helped to clarifying and improve the manuscript. Dr. Andrés Folguera is thanked for effective editorial handling. The authors are grateful to the National University of San

Juan and to CONICET. Authors acknowledge the use of the Matplotlib Python library (Hunter, 2007) and Quantum Geographical Information System (QGIS) (TEAM et al., 2014).

References

Aitcheson, S., Harmon, R., Moorbath, S., Schneider, A., Soler, P., Soria-Escalante, E., Steele, G., Swainbank, I., Wörner, G., 1995. Pb isotopes define basement domains of the altiplano, central andes. Geology 23, 555–558.

Allmendinger, R., Gubbels, T., 1996. Pure and simple shear plateau uplift, altiplano-puna, argentina and bolivia. Tectonophysics 259, 1–13.

Andersen, O., 2010. The dtu10 gravity field and mean sea surface, in: Second international symposium of the gravity field of the Earth (IGFS2), Fairbanks, Alaska, pp. 20–22.

Arnaiz-Rodríguez, M.S., Audemard, F., 2014. Variations in elastic thickness and flexure of the maracaibo block. Journal of South American Earth Sciences 56, 251–264.

Assumpção, M., Feng, M., Tassara, A., Julià, J., 2013. Models of crustal thickness for south america from seismic refraction, receiver functions and surface wave tomography. Tectonophysics 609, 82–96.

Audet, P., Bürgmann, R., 2011. Dominant role of tectonic inheritance in supercontinent cycles. Nature Geoscience 4, 184–187.

Babeyko, A.Y., Sobolev, S.V., Vietor, T., Oncken, O., Trumbull, R.B., 2006. Numerical study of weakening processes in the central andean back-arc, in: The Andes. Springer, pp. 495–512.

Baby, P., Rochat, P., Mascle, G., Hérail, G., 1997. Neogene shortening contribution to crustal thickening in the back arc of the central andes. Geology 25, 883–886.

588 Barnes, J., Ehlers, T., 2009. End member models for andean plateau uplift.
589 Earth-Science Reviews 97, 105–132.

590 Barthelmes, F., 2009. Definition of functionals of the geopotential and their
591 calculation from spherical harmonic models. http://publications. iass-
592 potsdam. de/pubman/item/escidoc 104132, 0902–2.

593 Beck, S.L., Zandt, G., 2002. The nature of orogenic crust in the central
594 andes. Journal of Geophysical Research: Solid Earth 107.

595 Beck, S.L., Zandt, G., Ward, K.M., Scire, A., 2015. Multiple styles and
596 scales of lithospheric foundering beneath the puna plateau, central andes.
597 Geological Society of America Memoirs 212, MWR212–03.

598 Bianucci, H., 1999. Estructura y evolución estructural del rift–relación con
599 la estratigrafía, subcuenca de lomas de olmedo (rama oriental), in: Relato-
600 rio XIV Congreso Geológico Argentino, Geología del Noroeste Argentino:
601 Salta, Asociación Geológica Argentina, pp. 292–300.

602 Blakely, R.J., 1995. Potential theory in gravity and magnetic applications.
603 Cambridge University Press.

604 Braitenberg, C., Ebbing, J., Götze, H.J., 2002. Inverse modelling of elastic
605 thickness by convolution method–the eastern alps as a case example. Earth
606 and Planetary Science Letters 202, 387–404.

607 Braitenberg, C., Zadro, M., 1999. Iterative 3d gravity inversion with inte-
608 gration of seismologic data. Boll. Geof. Teor. Appl 40, 4.

609 Brigham, E.O., 1974. The fast Fourier transform.

610 Brocher, T.M., 2005. Empirical relations between elastic wavespeeds and
611 density in the earth's crust. Bulletin of the Seismological Society of Amer-
612 ica 95, 2081–2092.

613 Brooks, B.A., Bevis, M., Whipple, K., Arrowsmith, J.R., Foster, J., Zap-
614 ata, T., Kendrick, E., Minaya, E., Echalar, A., Blanco, M., et al., 2011.

615 Orogenic-wedge deformation and potential for great earthquakes in the
616 central andean backarc. Nature Geoscience 4, 380.

617 Burov, E., Diament, M., 1996. Isostasy, equivalent elastic thickness, and
618 inelastic rheology of continents and oceans. Geology 24, 419–422.

619 Burov, E.B., Diament, M., 1995. The effective elastic thickness (t e) of
620 continental lithosphere: What does it really mean? Journal of Geophysical
621 Research: Solid Earth 100, 3905–3927.

622 Carrapa, B., DeCelles, P.G., 2015. Regional exhumation and kinematic his-
623 tory of the central andes in response to cyclical orogenic processes. Geo-
624 logical Society of America Memoirs 212, 201–213.

625 Chulick, G.S., Detweiler, S., Mooney, W.D., 2013. Seismic structure of the
626 crust and uppermost mantle of south america and surrounding oceanic
627 basins. Journal of South American Earth Sciences 42, 260–276.

628 Comínguez, A.H., Ramos, V.A., 1995. Geometry and seismic expression of
629 the cretaceous salta rift system, northwestern argentina .

630 Cristallini, E., Cominguez, A., Ramos, V., 1997. Deep structure of the metan-
631 guachipas region: Tectonic inversion in northwestern argentina. Journal
632 of South American Earth Sciences 10, 403–421.

633 Crosby, A., 2007. An assessment of the accuracy of admittance and coherence
634 estimates using synthetic data. Geophysical Journal International 171, 25–
635 54.

636 Deng, Y., Zhang, Z., Fan, W., Pérez-Gussinyé, M., 2014. Multitaper spectral
637 method to estimate the elastic thickness of south china: implications for
638 intracontinental deformation. Geoscience Frontiers 5, 193–203.

639 Dewey, J., Ryan, P., Andersen, T., 1993. Orogenic uplift and collapse, crustal
640 thickness, fabrics and metamorphic phase changes: the role of eclogites.
641 Geological Society, London, Special Publications 76, 325–343.

642 Dorbath, C., Granet, M., Poupinet, G., Martinez, C., 1993. A teleseismic
643 study of the altiplano and the eastern cordillera in northern bolivia: new
644 constraints on a lithospheric model. Journal of Geophysical Research: Solid
645 Earth 98, 9825–9844.

646 Featherstone, W., 1997. On the use of the geoid in geophysics: a case study
647 over the north west shelf of australia. Exploration Geophysics 28, 52–57.

648 Feng, M., Van der Lee, S., Assumpção, M., 2007. Upper mantle structure
649 of south america from joint inversion of waveforms and fundamental mode
650 group velocities of rayleigh waves. Journal of Geophysical Research: Solid
651 Earth 112.

652 Förste, C., Bruinsma, S., Abrikosov, O., Flechtner, F., Marty, J.C., Lemoine,
653 J.M., Dahle, C., Neumayer, H., Barthelmes, F., König, R., et al., 2014.
654 Eigen-6c4-the latest combined global gravity field model including goce
655 data up to degree and order 1949 of gfz potsdam and grgs toulouse, in:
656 EGU General Assembly Conference Abstracts. URL: `http://doi.org/`
657 `10.5880/icgem.2015.1`.

658 Förste, C., Flechtner, F., Schmidt, R., Meyer, U., Stubenvoll, R., Barthelmes,
659 F., König, R., Neumayer, K., Rothacher, M., Reigber, C., et al., 2005. A
660 new high resolution global gravity field model derived from combination of
661 grace and champ mission and altimetry/gravimetry surface gravity data,
662 in: Poster presented at EGU General Assembly, pp. 24–29.

663 Forsyth, D.W., 1985. Subsurface loading and estimates of the flexural rigidity
664 of continental lithosphere. Journal of Geophysical Research: Solid Earth
665 90, 12623–12632.

666 Garcia, E.S., Sandwell, D.T., Luttrell, K.M., 2015. An iterative spectral solu-
667 tion method for thin elastic plate flexure with variable rigidity. Geophysical
668 Journal International 200, 1012–1028.

669 Gardner, G., Gardner, L., Gregory, A., 1974. Formation velocity and den-
670 sity—the diagnostic basics for stratigraphic traps. Geophysics 39, 770–780.

Garzione, C.N., Molnar, P., Libarkin, J.C., MacFadden, B.J., 2006. Rapid late miocene rise of the bolivian altiplano: Evidence for removal of mantle lithosphere. Earth and Planetary Science Letters 241, 543–556.

Giese, P., Scheuber, E., Schilling, F., Schmitz, M., Wigger, P., 1999. Crustal thickening processes in the central andes and the different natures of the moho-discontinuity. Journal of South American Earth Sciences 12, 201–220.

Gómez-Ortiz, D., Agarwal, B.N., 2005. 3dinver. m: a matlab program to invert the gravity anomaly over a 3d horizontal density interface by parker–oldenburg's algorithm. Computers & geosciences 31, 513–520.

Hamza, V.M., Dias, F.J.S., Gomes, A.J., Terceros, Z.G.D., 2005. Numerical and functional representations of regional heat flow in south america. Physics of the Earth and Planetary Interiors 152, 223–256.

Hunter, J.D., 2007. Matplotlib: A 2d graphics environment. Computing In Science & Engineering 9, 90–95. URL: `https://matplotlib.org`.

Jacobsen, B.H., 1987. A case for upward continuation as a standard separation filter for potential-field maps. Geophysics 52, 1138–1148.

Jekeli, C., Yang, H.J., Ahlgren, K., 2013. Using isostatic gravity anomalies from spherical harmonic models and elastic plate compensation to interpret the lithosphere of the bolivian andes. Geophysics .

Jones, E., Oliphant, T., Peterson, P., 2001. SciPy: Open source scientific tools for Python. URL: `http://www.scipy.org/`.

Kane, M., 1962. A comprehensive system of terrain corrections using a digital computer. Geophysics 27, 455–462.

Karner, G., Watts, A., 1983. Gravity anomalies and flexure of the lithosphere at mountain ranges. Journal of Geophysical Research: Solid Earth 88, 10449–10477.

Kay, R.W., Kay, S.M., 1993. Delamination and delamination magmatism. Tectonophysics 219, 177–189.

Kay, S.M., Coira, B., Viramonte, J., 1994. Young mafic back arc volcanic rocks as indicators of continental lithospheric delamination beneath the argentine puna plateau, central andes. Journal of Geophysical Research: Solid Earth 99, 24323–24339.

Kay, S.M., Coira, B.L., 2009. Shallowing and steepening subduction zones, continental lithospheric loss, magmatism, and crustal flow under the central andean altiplano-puna plateau. Geological Society of America Memoirs 204, 229–259.

Kirby, J., Swain, C., 2004. Global and local isostatic coherence from the wavelet transform. Geophysical research letters 31.

Kirby, J., Swain, C., 2011. Improving the spatial resolution of effective elastic thickness estimation with the fan wavelet transform. Computers & geosciences 37, 1345–1354.

Kirby, J.F., 2014. Estimation of the effective elastic thickness of the lithosphere using inverse spectral methods: The state of the art. Tectonophysics 631, 87–116.

Kley, J., Monaldi, C., Salfity, J., 1999. Along-strike segmentation of the andean foreland: causes and consequences. Tectonophysics 301, 75–94.

Kley, J., Monaldi, C.R., 1998. Tectonic shortening and crustal thickness in the central andes: How good is the correlation? Geology 26, 723–726.

Kley, J., Monaldi, C.R., 2002. Tectonic inversion in the santa barbara system of the central andean foreland thrust belt, northwestern argentina. Tectonics 21.

Krystopowicz, N.J., Currie, C.A., 2013. Crustal eclogitization and lithosphere delamination in orogens. Earth and Planetary Science Letters 361, 195–207.

Lamb, S., Hoke, L., 1997. Origin of the high plateau in the central andes, bolivia, south america. Tectonics 16, 623–649.

Mantovani, M.S., Shukowsky, W., de Freitas, S.R., 1999. Tectonic pattern of south america inferred from tidal gravity anomalies. Physics of the earth and planetary interiors 114, 91–98.

Mantovani, M.S., Shukowsky, W., de Freitas, S.R., Neves, B.B.B., 2005. Lithosphere mechanical behavior inferred from tidal gravity anomalies: a comparison of africa and south america. Earth and Planetary Science Letters 230, 397–412.

Mantovani, M.S.M., De Freitas, S., Shukowsky, W., 2001. Tidal gravity anomalies as a tool to measure rheological properties of the continental lithosphere: Application to the south american plate. Journal of South American Earth Sciences 14, 1–14.

McKenzie, D., 2003. Estimating te in the presence of internal loads. Journal of Geophysical Research: Solid Earth 108.

McKenzie, D., Yi, W., Rummel, R., 2014. Estimates of te from goce data. Earth and Planetary Science Letters 399, 116–127.

Mengel, K., Kern, H., 1992. Evolution of the petrological and seismic moho-implications for the continental crust-mantle boundary. Terra Nova 4, 109–116.

Mouthereau, F., Watts, A.B., Burov, E., 2013. Structure of orogenic belts controlled by lithosphere age. Nature geoscience 6, 785.

Myers, S.C., Beck, S., Zandt, G., Wallace, T., 1998. Lithospheric-scale structure across the bolivian andes from tomographic images of velocity and attenuation for p and s waves. Journal of Geophysical Research: Solid Earth 103, 21233–21252.

Nagy, D., 1966. The gravitational attraction of a right rectangular prism. Geophysics 31, 362–371.

754 Oldenburg, D.W., 1974. The inversion and interpretation of gravity anoma-
755 lies. Geophysics 39, 526–536.

756 Pacino, M., Introcaso, A., 1987. Regional anomaly determination using the
757 upwards-continuation method. Bollettino di Geofisica Teorica ed Applicata
758 29, 113–122.

759 Parker, R., 1973. The rapid calculation of potential anomalies. Geophysical
760 Journal International 31, 447–455.

761 Pavlis, N.K., Holmes, S.A., Kenyon, S.C., Factor, J.K., 2008. An earth
762 gravitational model to degree 2160: Egm2008. EGU General Assembly
763 2008, 4–2.

764 Pavlis, N.K., Holmes, S.A., Kenyon, S.C., Factor, J.K., 2012. The devel-
765 opment and evaluation of the earth gravitational model 2008 (egm2008).
766 Journal of Geophysical Research: Solid Earth 117.

767 Pérez-Gussinyé, M., Lowry, A., Phipps Morgan, J., Tassara, A., 2008. Ef-
768 fective elastic thickness variations along the andean margin and their rela-
769 tionship to subduction geometry. Geochemistry, Geophysics, Geosystems
770 9.

771 Pérez-Gussinyé, M., Lowry, A., Watts, A., 2007. Effective elastic thickness of
772 south america and its implications for intracontinental deformation. Geo-
773 chemistry, Geophysics, Geosystems 8.

774 Pérez-Gussinyé, M., Swain, C., Kirby, J., Lowry, A., 2009. Spatial variations
775 of the effective elastic thickness, te, using multitaper spectral estimation
776 and wavelet methods: examples from synthetic data and application to
777 south america. Geochemistry, Geophysics, Geosystems 10.

778 Pérez-Gussinyé, M., Watts, A., 2005. The long-term strength of europe and
779 its implications for plate-forming processes. Nature 436, 381–384.

780 Prezzi, C.B., Götze, H.J., Schmidt, S., 2009. 3d density model of the central
781 andes. Physics of the Earth and Planetary Interiors 177, 217–234.

Prezzi, C.B., Götze, H.J., Schmidt, S., 2014. Andean foreland evolution and flexure in nw argentina: Chaco–paraná basin. Tectonophysics 628, 228–243.

Sacek, V., Ussami, N., 2009. Reappraisal of the effective elastic thickness for the sub-andes using 3-d finite element flexural modelling, gravity and geological constraints. Geophysical Journal International 179, 778–786.

Sánchez, M.A., Ariza, J.P., García, H.P., Gianni, G.M., Weidmann, M.C., Folguera, A., Klinger, F.L., Martinez, M.P., 2017. Thermo-mechanical analysis of the andean lithosphere over the chilean-pampean flat-slab region. Journal of South American Earth Sciences .

Sandwell, D.T., Smith, W.H.F., 2009. Global marine gravity from retracked geosat and ers-1 altimetry: Ridge segmentation versus spreading rate. Journal of Geophysical Research: Solid Earth 114. URL: http://dx.doi.org/10.1029/2008JB006008. b01411.

Silver, P.G., Russo, R.M., Lithgow-Bertelloni, C., 1998. Coupling of south american and african plate motion and plate deformation. Science 279, 60–63.

Simons, F.J., van der Hilst, R.D., Zuber, M.T., 2003. Spatiospectral localization of isostatic coherence anisotropy in australia and its relation to seismic anisotropy: Implications for lithospheric deformation. Journal of Geophysical Research: Solid Earth 108.

Sobolev, S.V., Babeyko, A.Y., 2005. What drives orogeny in the andes? Geology 33, 617–620.

Sobolev, S.V., Babeyko, A.Y., Koulakov, I., Oncken, O., 2006. Mechanism of the andean orogeny: insight from numerical modeling, in: The Andes. Springer, pp. 513–535.

Soler, S.R., 2015. Métodos espectrales para la determinación de la profundidad del punto de curie y el espesor elástico de la corteza terrestre. Degree thesis. Facultad de Ciencias Exactas, Ingeniería y Agrimensura Uni-

versidad Nacional de Rosario, Argentina. URL: https://github.com/santis19/tesina-fisica.

Stewart, J., Watts, A., 1997. Gravity anomalies and spatial variations of flexural rigidity at mountain ranges. Journal of Geophysical Research: Solid Earth 102, 5327–5352.

Swain, C., Kirby, J., 2006. An effective elastic thickness map of australia from wavelet transforms of gravity and topography using forsyth's method. Geophysical research letters 33.

Tassara, A., 2005. Interaction between the nazca and south american plates and formation of the altiplano–puna plateau: Review of a flexural analysis along the andean margin (15–34 s). Tectonophysics 399, 39–57.

Tassara, A., Echaurren, A., 2012. Anatomy of the andean subduction zone: three-dimensional density model upgraded and compared against global-scale models. Geophysical Journal International 189, 161–168.

Tassara, A., Götze, H.J., Schmidt, S., Hackney, R., 2006. Three-dimensional density model of the nazca plate and the andean continental margin. Journal of Geophysical Research: Solid Earth 111.

Tassara, A., Swain, C., Hackney, R., Kirby, J., 2007. Elastic thickness structure of south america estimated using wavelets and satellite-derived gravity data. Earth and Planetary Science Letters 253, 17–36.

Tassara, A., Yáñez, G., 2003. Relación entre el espesor elástico de la litosfera y la segmentación tectónica del margen andino (15-47 s). Revista geológica de Chile 30, 159–186.

TEAM, Q.D., et al., 2014. Quantum gis geographic information system. open source geospatial foundation project.

Turcotte, D., Schubert, G., 2002. Geodynamics, 456 pp.

837 Uieda, L., Barbosa, V.C., 2017. Fast nonlinear gravity inversion in spherical
838 coordinates with application to the south american moho. Geophysical
839 Journal International 208, 162–176.

840 Uieda, L., Oliveira Jr, V., Ferreira, A., Santos, H., Caparica Jr, J., 2014. Fa-
841 tiando a terra: A python package for modeling and inversion in geophysics:
842 figshare. URL: `http://www.fatiando.org`.

843 Watts, A., 1978. An analysis of isostasy in the world's oceans 1. hawaiian-
844 emperor seamount chain. Journal of Geophysical Research: Solid Earth
845 83, 5989–6004.

846 Watts, A., Burov, E., 2003. Lithospheric strength and its relationship to
847 the elastic and seismogenic layer thickness. Earth and Planetary Science
848 Letters 213, 113–131.

849 Watts, A., Lamb, S., Fairhead, J., Dewey, J., 1995. Lithospheric flexure and
850 bending of the central andes. Earth and Planetary Science Letters 134,
851 9–21.

852 Watts, A.B., 2001. Isostasy and Flexure of the Lithosphere. Cambridge
853 University Press.

854 Wienecke, S., Braitenberg, C., Götze, H.J., 2007. A new analytical solution
855 estimating the flexural rigidity in the central andes. Geophysical Journal
856 International 169, 789–794.

857 Wigger, P.J., Schmitz, M., Araneda, M., Asch, G., Baldzuhn, S., Giese,
858 P., Heinsohn, W.D., Martínez, E., Ricaldi, E., Röwer, P., et al., 1994.
859 Variation in the crustal structure of the southern central andes deduced
860 from seismic refraction investigations, in: Tectonics of the southern Central
861 Andes. Springer, pp. 23–48.

862 Yuan, X., Sobolev, S., Kind, R., 2002. Moho topography in the central andes
863 and its geodynamic implications. Earth and Planetary Science Letters 199,
864 389–402.

865 Yuan, X., Sobolev, S.V., Kind, R., Oncken, O., et al., 2000. Subduction and
866 collision processes in the central andes constrained by converted seismic
867 phases. Nature 408, 958.

Highlights

Gravity inversion to obtain the geometry of Moho in The Central Andes of South America.

Determination of effective elastic thickness from a high resolution gravity dataset (Eigen-6C4 model).

Correlation between styles and mechanisms of deformation in the easternmost sector of the Central Andes and the elastic thickness.

Inverse correlation between the elastic thickness and heat flow.

Shallower gravity Moho linked to a high-gravity anomaly and a high-velocity in the uppermost mantle.